IEEE Access
Multidisciplinary ⋮ Rapid Review ⋮ Open Access Journal

Received May 26, 2020, accepted June 5, 2020, date of publication June 9, 2020, date of current version June 23, 2020.

Digital Object Identifier 10.1109/ACCESS.2020.3001186

Control Design for the Autonomous Horizontal Takeoff Phase of the Reusable Launch Vehicles

SHUAIBIN AN[1,2], KAI LIU[1,2], (Member, IEEE), YAZHUO FAN[3], JIAN GUO[3], AND ZHIYONG SHE[3]

[1]Laboratory of Advanced Technology for Aerospace Vehicles, Dalian University of Technology, Dalian 116024, China
[2]Department of Aeronautics and Astronautics, Dalian University of Technology, Dalian 116024, China
[3]Beijing Institute of Aerospace Technology, Beijing 100074, China

Corresponding author: Kai Liu (carsonliu@dlut.edu.cn)

This work was supported by the National Natural Science Foundation of China (NSFC) under Grant 61603363, Grant 61703383, and Grant 61603056.

ABSTRACT The control system design for the reusable launch vehicles (RLVs), especially in the autonomous horizontal takeoff phase, is a highly challenging task. Significant issues arise due to the high nonlinearity, large uncertainties of aerodynamic coefficients as well as strong coupling among axes of the airframe. This paper studies autonomous takeoff control problem of the RLVs by the means of trajectory linearization control (TLC) and model predictive control (MPC) theory. The six degree of freedom dynamic model is firstly established, and the flight strategy of takeoff and climb stage is provided through the characteristic analysis of RLVs. Furthermore, the guidance law for the climbing phase is proposed via the TLC method against the high nonlinearity, and a speed based gain-schedule strategy is given under the consideration of both aerodynamic force and friction force. In order to eliminate the ground effect interference, an improved model predictive control approach is presented by introducing the online parameter estimation of the ground effect interaction coefficient, and a coupled model predictive controller is designed by introducing the feedback of sideslip angle into the roll control channel to eliminate the coupling effect. Finally, the performance of the design method for autonomous takeoff control of RLVs is demonstrated through the comparison simulation analysis.

INDEX TERMS Reusable launch vehicles, hypersonic vehicles, model predictive control, trajectory linearization control.

I. INTRODUCTION

Aiming at the development of more affordable, convenient and reliable access to space, the reusable launch vehicles (RLVs) [1]–[9], such as space rider [10] and Skylon [11] have become a hot spot and received sustained attention during the last few decades. The RLVs will dramatically reduce the operational cost of space missions because they can be used repeatedly by quick recovering and reusing after each space mission.

Compared with the hypersonic cruise vehicle [12], [13], the RLVs should not only adapt to the near space flight environment, but also meet the technical requirements of the airport Horizontal takeoff and landing. The small wing area of the aircraft is beneficial to reduce the drag when the aircraft is flying at high speed. In contrast, aviation aircraft often use large airfoils. Therefore, compared with aircraft such as fighter and airliner, its low-speed lift performance is poor. At the same time, in order to meet the needs of high and low-speed, the design of a combined power engine is usually poor at subsonic speeds, so the horizontal takeoff and landing process will face the problem of insufficient lift performance and thrust performance, and the autonomous takeoff control technology will face new challenges.

In recent years, many scholars have done a lot of research on the takeoff control of aircraft. Hypersonic aircraft often use small wing surfaces instead of traditional wing surfaces to improve maneuverability [14], [15]. In order to achieve rapid orbit entry, the takeoff angle of attack often reaches a large angle of attack range. In this case, a very complex asymmetric vortex will form in the leeward region of the aircraft, which will have a great impact on the aerodynamic characteristics of the aircraft and may lead to the failure of the aircraft launch. The traditional proportional integral

The associate editor coordinating the review of this manuscript and approving it for publication was Nasim Ullah.

differential (PID) controller can't achieve satisfactory effect either in the setting of control coefficient or in the control effect. Based on the classical PID control structure, the horizontal and vertical control laws of the sliding section are designed, but the constant coefficient controller is difficult to meet the needs of the whole sliding process [16]. To solve the problem that the traditional PID cannot meet the quality control during the whole flight, a longitudinal nonlinear takeoff control strategy is proposed [17]. In addition, fuzzy PID is useful in correcting sideslip, but the design of fuzzy control law often needs a lot of experience data [18]. Moreover, a nonlinear controller is designed to track the command signal of pitch angle rate formulated by the designer, and the restrictions of elevator deflection angle and elevator deflection rate are considered [19]. Furthermore, different delay time in the multi delay model(MDM) represents high-frequency uncertainty, and the multi design point(MDP) method is used to simulate the parameter change caused by the change of flight state; combined with MDM/MDP method, the general control structure is selected and the optimal control is used to select the parameters [20].

It can be found that the above guidance and control schemes are mainly applied to subsonic and supersonic vehicles, while the research on RLVs with lift body is less at present. Therefore, this paper studies the design method of takeoff guidance and control for RLVs. Model predictive control (MPC) is used to track and control the trajectory of intelligent vehicle [21], and has achieved good control effect. Its basic idea is to use the system model to predict the future state of the system, and introduce the prediction error of the future time into the solution of the current time control command. MPC has high control accuracy. Thus, for the control of the takeoff phase of RLVs, a design method of the takeoff control law based on the MPC theory is proposed. In particular, an improve model predictive control (IMPC) method is proposed, which corrects the solution of control instruction by introducing the on-line parameter estimation of ground effect uncertainty coefficient. TLC method [22]–[24] first uses the pseudo dynamic inverse of the open-loop of the controlled object to transform the trajectory tracking problem into a nonlinear time-varying tracking error regulation problem, and then designs a closed-loop state feedback control law to make the whole system obtain satisfactory control performance. At present, TLC method has been successfully used in missile, flight control simulation platform, mobile robot and no-minimum phase system design, and achieved good control effect. At the same time, TLC, as one of the alternatives of NASA's advanced guidance and control methods, has designed an excellent flight control system for the X-33 aircraft.

This paper is divided into the following parts: the second part analyzes the dynamic characteristics of the hypersonic vehicle in the takeoff stage, and establishes the dynamic model of the vehicle. The third part decouples the aircraft dynamics model, the longitudinal channel design TLC guidance law, the lateral channel design PID correction guidance law. The fourth part derives the MPC attitude control law, in particular, gives the form of IMPC and the lateral-heading coupling MPC. In the fifth part, the simulation of the guidance and control of the aircraft takeoff is completed, and the simulation results of the improved controller and the original controller are compared to verify the effectiveness of the guidance and control design. The sixth part summarizes the simulation results and draws a conclusion.

II. DYNAMICS MODELING AND TRAJECTORY DESIGN

A. DYNAMIC MODEL

According to the conversion relationship between the body coordinate system and the ground coordinate system, the attitude dynamic model of RLVs in the takeoff stage can be established. The six-degree-of-freedom dynamics equation is as (1), shown at the bottom of the next page.

where variables are represented as follows: $\alpha, \beta, \gamma_V, \psi_V$ are angle of attack, sideslip angle, roll angle, and trajectory deflection angle; ϑ, ψ, γ are pitch angle, yaw angle and roll angle; $\omega x, \omega y, \omega z$ are roll, pitch, and yaw angular rates; D, L, Z, f are drag, lift, lateral force and friction; Mx, My, Mz are the aerodynamic moment of roll, yaw and pitch; Mn, Mf are the ground support moment, friction moment, $Mnx, Mfx, Mny, Mfy, Mnz, Mfz$ represent the projection of the above moment under the body coordinate axis; Jx, Jy, Jz are roll, yaw, and pitch torques of inertial; V, m, g, θ are velocity, vehicle mass, gravity acceleration, the flight path angle; T, Isp are engine thrust and specific impulse; H, Y, X are the altitude, side distance and heading distance.

During the running process, according to the contact between the landing gear and the ground, the supporting force on the landing gear is different. Support analysis is as follows:

$$\bar{\boldsymbol{P}}^{\boldsymbol{e}} = \begin{bmatrix} P^e_{px} \\ P^e_{py} \\ P^e_{pz} \end{bmatrix} = \begin{cases} \begin{bmatrix} 0 \\ P_n + P_{ml} + P_{mr} \\ 0 \end{bmatrix} & Three - wheel \\ \begin{bmatrix} 0 \\ P_{ml} + P_{mr} \\ 0 \end{bmatrix} & Two - wheel \end{cases} \tag{2}$$

In the formula, Pn is for front wheel support, Pml, Pmr are the support force of the left and right main landing gear, In the body coordinate system, The resultant moment vector caused by $\bar{\boldsymbol{P}}^{\boldsymbol{e}}$ force on the aircraft is as follows:

$$\begin{aligned} \boldsymbol{M_n} &= \begin{bmatrix} M^b_{px} \\ M^b_{py} \\ M^b_{pz} \end{bmatrix} \\ &= \begin{cases} \begin{bmatrix} (P_{ml} - P_{mr}) \cdot b_w/2 \\ 0 \\ P_n \cdot a_n - (P_{ml} + P_{mr}) \cdot a_m \end{bmatrix} & Three - wheel \\ \begin{bmatrix} (P_{ml} - P_{mr}) \cdot b_w/2 \\ 0 \\ -(P_{ml} + P_{mr}) \cdot a_m \end{bmatrix} & Two - whell \end{cases} \end{aligned} \tag{3}$$

where, *bw* is distance between main wheels, *an* is the vertical distance projected from the front wheel to the center of gravity, *am* is the vertical distance projected from the main wheel to the center of gravity.

Since the track and the landing gear are not smooth, the landing gear is subject to friction with the track. Its numerical form and vector form are as equation (4) (5):

$$\begin{cases} Q_n = \mu_{pnx} \cdot P_n \\ Q_{ml} = \mu_{pmlx} \cdot P_{ml} \\ Q_{mr} = \mu_{pmrx} \cdot P_{mr} \end{cases} \tag{4}$$

$$\bar{\boldsymbol{Q}}^{\boldsymbol{e}} = \begin{bmatrix} Q^e_{px} \\ Q^e_{py} \\ Q^e_{pz} \end{bmatrix} = \begin{bmatrix} -(Q_n + Q_{ml} + Q_{mr}) \\ 0 \\ 0 \end{bmatrix} \tag{5}$$

μpnx, $\mu pmlx$, $\mu pmrx$ are the longitudinal friction coefficients of the front wheels and the left and right main landing gear wheels. The resultant moment vector caused by $\bar{\boldsymbol{Q}}^{\boldsymbol{e}}$ force on the aircraft is as follows:

$$\boldsymbol{M_f} = \begin{cases} \begin{bmatrix} Q_n \sin\theta_L \cdot h_1 \\ 1/2(Q_{ml} - Q_{mr}) \cdot b_w + a_n \sin\theta_L Q_n \\ -Q_n \cos\theta_L \cdot h_1 - (Q_{ml} + Q_{mr}) \cdot h_2 \end{bmatrix} & Three - wheel \\ \begin{bmatrix} 0 \\ (Q_{ml} - Q_{mr}) b_w/2 \\ -(Q_{ml} + Q_{mr}) \cdot h_2 \end{bmatrix} & Two - wheel \end{cases} \tag{6}$$

Among, θL is the front wheel declination.

B. NOMINAL FLIGHT PATH DESIGN

According to the force of the takeoff section, the takeoff of the hypersonic aircraft is divided into three phases: three-wheel

$$\begin{aligned}
\frac{d\omega_x}{dt} &= \frac{(J_y - J_z)}{J_x}\omega_z\omega_y + \frac{M_x + M_{nx} + M_{fx}}{J_x} \\
\frac{d\omega_y}{dt} &= \frac{(J_z - J_x)}{J_y}\omega_x\omega_z + \frac{M_y + M_{ny} + M_{fy}}{J_y} \\
\frac{d\omega_z}{dt} &= \frac{(J_x - J_y)}{J_z}\omega_x\omega_y + \frac{M_z + M_{nz} + M_{fz}}{J_z} \\
\frac{d\vartheta}{dt} &= \omega_y \sin\gamma + \omega_z \cos\gamma \\
\frac{d\psi}{dt} &= \frac{\omega_y \cos\gamma - \omega_z \sin\gamma}{\cos\vartheta} \\
\frac{d\gamma}{dt} &= \omega_x - \tan\vartheta(\omega_y \cos\gamma - \omega_z \sin\gamma) \\
\frac{d\theta}{dt} &= \frac{T(\sin\alpha\cos\gamma_V - \cos\alpha\sin\beta\sin\gamma_V) + L\cos\gamma_V - Z\sin\gamma_V}{mV} - \frac{g\cos\theta}{V} \\
\frac{d\psi_V}{dt} &= -\frac{T(\sin\alpha\sin\gamma_V - \cos\alpha\sin\beta\cos\gamma_V) + L\sin\gamma_V + Z\cos\gamma_V}{mV\cos\theta} \\
\sin\gamma_V &= \frac{(\cos\alpha\sin\beta\sin\vartheta - \sin\alpha\sin\beta\cos\gamma\cos\vartheta + \cos\beta\sin\gamma\cos\vartheta)}{\cos\theta} \\
\sin\beta &= \cos\theta[\cos\gamma\sin(\psi - \psi_V) + \sin\vartheta\sin\gamma\cos(\psi - \psi_V)] - \sin\theta\cos\vartheta\sin\gamma \\
\sin\alpha &= \frac{\cos\theta[-\sin\gamma\sin(\psi - \psi_V) + \sin\vartheta\cos\gamma\cos(\psi - \psi_V)] - \sin\theta\cos\vartheta\cos\gamma}{\cos\beta} \\
\frac{dV}{dt} &= \frac{T\cos\alpha\cos\beta - D - mg\sin\theta - f}{m} \\
\frac{dH}{dt} &= V\sin\theta \\
\frac{dY}{dt} &= -V\cos\theta\sin\psi_V \\
\frac{dX}{dt} &= V\cos\theta\cos\psi_V \\
\frac{dm}{dt} &= -\frac{T}{Isp \cdot g}
\end{aligned} \tag{1}$$

skating, two-wheel skating, and aerial climb. As shown in the figure below:

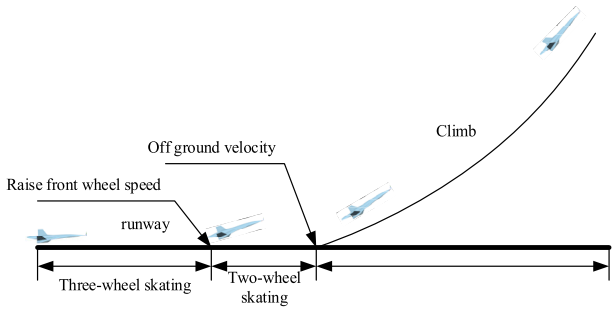

FIGURE 1. Schematic diagram of aircraft takeoff process.

In the three-wheeled skating section, the aircraft accelerates on the runway with the engine at a fixed stopping angle. At this time, the moment of the pitch channel should be balanced and the aircraft is on the runway centerline.

In the two-wheel skating section, when the aircraft is accelerated to a certain speed, the aerodynamic pitching moment is sufficient to lift the front wheel of the aircraft off the ground. When the pitch angle is raised to the climb angle, the engine is continuously turned on to continue acceleration until the aircraft lift is greater than gravity and takes off from the ground.

In the takeoff and climb section, according to the current climbing strategy of the aircraft, the RLVs climbs to a safe altitude at a fixed pitch angle.

C. SYSTEM DECOUPLING

During take-off, without considering the lateral deviation, the lateral—heading state $\omega x, \omega y, \psi, \psi_V, \gamma, \gamma_V, \beta, Y, X$ quantity changes little, the lateral state point is 0 at most state points, and the longitudinal state $\omega z, \alpha, \vartheta, \theta, V, H$ becomes the main influencing factor of the dynamic equation [27]. Therefore, consider decoupling the lateral and longitudinal directions to design guidance control algorithms separately. Let the lateral state quantity in equation (1) be equal to 0 to obtain the longitudinal motion equations:

$$\begin{aligned}
\frac{d\omega_z}{dt} &= \frac{M_z + M_{nz} + M_{fz}}{J_z} \\
\frac{d\vartheta}{dt} &= \omega_z \\
\frac{d\theta}{dt} &= \frac{T\sin\alpha + L}{mV} - \frac{g\cos\theta}{V} \\
\alpha &= \vartheta - \theta \\
\frac{dV}{dt} &= \frac{T\cos\alpha - D - mg\sin\theta - f}{m} \\
\frac{dH}{dt} &= V\sin\theta \\
\frac{dm}{dt} &= -\frac{T}{Isp\cdot g}
\end{aligned} \tag{7}$$

Among them, the input of the longitudinal system is T, Mz, Mnz, Mfz. Subsequently, the equation of lateral—heading can also be obtained (8), as shown at the bottom of the next page.

Among them, the input of the lateral—heading system is $T, Mx, Mnx, Mfx, My, Mny, Mfy$.

III. DESIGN OF GUIDANCE LAW FOR TAKEOFF

During take-off, the longitudinal subsystem includes three different flight states. Its state value quantity changes in a large range and has strong nonlinearity. The essence of trajectory linearization guidance is to update PID coefficients in real time, which can solve the problem of strong nonlinearity. The state quantity of the lateral subsystem changes little, basically near the zero-balance point, and the traditional PID can solve the guidance design problem well. Therefore, this section presents two different guidance schemes, one for the longitudinal subsystem and the other for the lateral-heading subsystem.

A. DESIGN OF LONGITUDINAL GUIDANCE LAW BASED ON TLC

1) TRAJECTORY TRACKING GUIDANCE VIA TLC

According to the six degree of freedom dynamic model of the aircraft, the dynamic equation of the pitching channel of the aircraft is as follows:

$$\begin{cases}
\dfrac{dV}{dt} = \dfrac{T\cos\alpha - D}{m} - g\sin\theta \\
\dfrac{d\theta}{dt} = \dfrac{T\sin\alpha\cos\gamma + L\cos\gamma}{mV} - \dfrac{g\cos\theta}{V} \\
\dfrac{dh}{dt} = V\sin\theta \\
\dfrac{dm}{dt} = -\dfrac{T}{Isp\cdot g}
\end{cases} \tag{9}$$

where V, θ, h, m represent four state variables of aircraft speed, trajectory inclination, altitude and mass, T, D, L indicate thrust, resistance and lift, α, kk mean angle of attack and rocket flow.

In order to facilitate the design of guidance law, velocity and altitude are taken as state variables, and $\int V, \dot{h}$ is introduced to expand the dimension of the model (10), as shown at the bottom of the next page..

Put the equation of state into the form of error equation of state. The input to the system is $\tilde{\boldsymbol{u}} = [\,\alpha \;\; kk\,]^T$, State value $\boldsymbol{e} = [\,\Delta\int V \;\; \Delta V \;\; \Delta h \;\; \Delta\frac{dh}{dt}\,]^T$, which represents the error between the theoretical value and the true value.

$$\begin{aligned}
\dot{\boldsymbol{e}}(t) &= \boldsymbol{A}(t)\boldsymbol{e}(t) + \boldsymbol{B}(t)\tilde{\boldsymbol{u}}(t) \\
\boldsymbol{A}(t) &= \boldsymbol{A}(\bar{\boldsymbol{x}}, \bar{\boldsymbol{u}}) = \left(\frac{\partial \boldsymbol{f}}{\partial \boldsymbol{x}}\right)\Big|_{\bar{\boldsymbol{x}},\bar{\boldsymbol{u}}} = \begin{pmatrix} 0 & 1 & 0 & 0 \\ 0 & a_{22} & a_{23} & 0 \\ 0 & 0 & 0 & 1 \\ 0 & a_{42} & a_{43} & 0 \end{pmatrix}\Bigg|_{\bar{\boldsymbol{x}},\bar{\boldsymbol{u}}} \\
\boldsymbol{B}(t) &= \boldsymbol{B}(\bar{\boldsymbol{x}}, \bar{\boldsymbol{u}}) = \left(\frac{\partial \boldsymbol{f}}{\partial u}\right)\Big|_{\bar{\boldsymbol{x}},\bar{\boldsymbol{u}}} = \begin{pmatrix} 0 & 0 \\ b_{21} & b_{22} \\ 0 & 0 \\ b_{41} & b_{42} \end{pmatrix}\Bigg|_{\bar{\boldsymbol{x}},\bar{\boldsymbol{u}}}
\end{aligned} \tag{11}$$

In equation (11), the meaning of the coefficient is as (12), shown at the bottom of the next page.

2) CONTROL LAW DESIGN

The obtained linear time-varying error system can adopt the following form of time-varying controller.

$$\tilde{\boldsymbol{u}}(t) = \boldsymbol{K}(t)\boldsymbol{e}(t) \tag{13}$$

Simultaneous equation (13) and equation (11) to obtain the state matrix of the closed-loop system. The matrix of closed-loop system is in the following form:

$$\boldsymbol{Acl}(t) = \boldsymbol{A}(t) + \boldsymbol{B}(t)\boldsymbol{K}(t) \tag{14}$$

The expected closed-loop matrix is:

$$\boldsymbol{A_r}(t) = \begin{pmatrix} 0 & 1 & 0 & 0 \\ \lambda_1 & \lambda_2 & 0 & 0 \\ 0 & 0 & 0 & 1 \\ 0 & 0 & \lambda_3 & \lambda_4 \end{pmatrix} \tag{15}$$

$$\begin{aligned}
\frac{d\omega_x}{dt} &= \frac{(J_y - J_z)}{J_x}\omega_z\omega_y + \frac{M_x + M_{nx} + M_{fx}}{J_x} \\
\frac{d\omega_y}{dt} &= \frac{(J_z - J_x)}{J_y}\omega_x\omega_z + \frac{M_y + M_{ny} + M_{fy}}{J_y} \\
\frac{d\psi}{dt} &= \frac{\omega_y \cos\gamma - \omega_z \sin\gamma}{\cos\vartheta} \\
\frac{d\gamma}{dt} &= \omega_x - \tan\vartheta(\omega_y \cos\gamma - \omega_z \sin\gamma) \\
\frac{d\psi_V}{dt} &= -\frac{T(\sin\alpha \sin\gamma_V - \cos\alpha \sin\beta \cos\gamma_V) + L\sin\gamma_V + Z\cos\gamma_V}{mV\cos\theta} \\
\sin\gamma_V &= \frac{(\cos\alpha \sin\beta \sin\vartheta - \sin\alpha \sin\beta \cos\gamma \cos\vartheta + \cos\beta \sin\gamma \cos\vartheta)}{\cos\theta} \\
\sin\beta &= \cos\theta[\cos\gamma \sin(\psi - \psi_V) + \sin\vartheta \sin\gamma \cos(\psi - \psi_V)] - \sin\theta \cos\vartheta \sin\gamma \\
\frac{dY}{dt} &= -V\cos\theta \sin\psi_V \\
\frac{dX}{dt} &= V\cos\theta \cos\psi_V
\end{aligned} \tag{8}$$

$$\begin{cases}
\dfrac{d\left(\int V\right)}{dt} = V \\
\dfrac{dV}{dt} = \dfrac{T\cos\alpha - D}{m} - g\sin\theta \\
\dfrac{dh}{dt} = V\sin\theta \\
\dfrac{d^2h}{dt^2} = \dfrac{(\cos\alpha \sin\theta + \cos\theta \sin\alpha \cos\gamma)\cdot T - \sin\theta \cdot D + \cos\theta \cos\gamma \cdot Y - mg}{m}
\end{cases} \tag{10}$$

$$\begin{aligned}
a_{22} &= \frac{\left(\frac{\partial T}{\partial V}\cos\alpha - \frac{\partial D}{\partial V}\right)}{m} \\
a_{23} &= \frac{\left(\frac{\partial T}{\partial h}\cos\alpha - \frac{\partial D}{\partial h}\right)}{m} \\
a_{42} &= \frac{\left[(\cos\alpha \sin\theta + \cos\theta \sin\alpha \cos\gamma)\frac{\partial T}{\partial V} - \sin\theta\frac{\partial D}{\partial V} + \cos\theta\cos\gamma\frac{\partial Y}{\partial V}\right]}{m} \\
a_{43} &= \frac{\left[(\cos\alpha \sin\theta + \cos\theta \sin\alpha \cos\gamma)\frac{\partial T}{\partial h} - \sin\theta\frac{\partial D}{\partial h} + \cos\theta\cos\gamma\frac{\partial Y}{\partial h}\right]}{m} \\
b_{21} &= \frac{\left(-T\sin\alpha - \frac{\partial D}{\partial \alpha}\right)}{m} \\
b_{22} &= \frac{\frac{\partial T}{\partial kk}\cos\alpha}{m} \\
b_{41} &= \frac{\left[(-\sin\alpha \sin\theta + \cos\theta\cos\alpha\cos\gamma)\cdot T - \sin\theta\frac{\partial D}{\partial \alpha} + \cos\theta\cos\gamma\frac{\partial Y}{\partial \alpha}\right]}{m} \\
b_{42} &= \frac{[\cos\alpha \sin\theta + \cos\theta \sin\alpha \cos\gamma]\frac{\partial T}{\partial kk}}{m}
\end{aligned} \tag{12}$$

Making equation (14) equals to equation (15), the time-varying controller matrix can be got:

$$\boldsymbol{K}(t) = \boldsymbol{B}(t)^{-1}[\boldsymbol{Acl}(t) - \boldsymbol{A}(t)] \tag{16}$$

The above control parameters are determined by the expected characteristic root, so the core problem is the selection of the expected characteristic root.

From the matrix of the expected closed-loop system, the three subspaces can be described as a linear time-varying second-order system, which is described as the form of the characteristic equation.

$$\begin{aligned} s^2 - \lambda_2(t)s - \lambda_1(t) = 0 \\ s^2 - \lambda_4(t)s - \lambda_3(t) = 0 \end{aligned} \tag{17}$$

Hence

$$\begin{aligned} \lambda_1(t) = -\omega_1(t)^2 \quad \lambda_2(t) = -2\varsigma_1(t)\omega_1(t) \\ \lambda_3(t) = -\omega_2(t)^2 \quad \lambda_4(t) = -2\varsigma_2(t)\omega_2(t) \end{aligned} \tag{18}$$

Here $\omega 1(t), \omega 2(t)$ represents the natural frequency, $\varsigma 1(t), \varsigma 2(t)$ represents the damping ratio. The natural frequency and damping ratio of the desired system can be determined by the demand performance (including rise time, overshoot), to design the controller parameters to meet the performance requirements.

The rise time and overshoot of underdamped second-order linear system for step response are estimated as follows:

$$t_r = \frac{\pi - \arccos\varsigma}{\omega\sqrt{1-\varsigma^2}} \tag{19}$$

$$\sigma = e^{-\pi\varsigma/\sqrt{1-\varsigma^2}} \times 100\% \tag{20}$$

The rise time and overshoot of the desired closed-loop control system can be given to solve the damping ratio and frequency of the desired system, then the eigenvalue of the desired system matrix can be determined and the controller parameters can be obtained.

3) PROOF OF STABILITY

Lemma 1: For closed-loop error linear time-varying system (11), if the characteristic value of the system [33]

$$\rho_{1,2}(t) = -(\zeta \pm j\sqrt{1-\zeta^2})\omega_n(t), \quad 0 < \zeta < 1 \tag{21}$$

satisfies:

1) There are constants c_1, c_2 satisfied:

$$\lim_{T\to\infty} \sup_{t_0>0} \frac{1}{T} \int_{t_0}^{t_0+T} \mathrm{Re}(\rho_k(\tau))d\tau = -c_k < 0, \quad k = 1, 2 \tag{22}$$

2) There is a positive integer m satisfied:

$$\lim_{t\to\infty} \frac{Im\rho_k(t)}{t^m} = 0, \quad k = 1, 2 \tag{23}$$

Then the time-varying closed-loop system is uniformly stable.

Using the above theorem to analyze the time-varying linear controller, the characteristic values of the closed-loop system after the TLC is added are:

$$\rho_{1,2}(t) = -(\zeta \pm j\sqrt{1-\zeta^2})\omega_n(t), \quad 0 < \zeta < 1$$

Then, if the normal number c exists:

$$\omega_n(t) > c > 0, \quad t > 0$$

Then obviously (22-23) are all established, the controller designed based on the above characteristic roots can ensure the stability of the closed-loop time-varying system.

B. DESIGN OF THE CROSS-HEADING GUIDANCE LAW

1) STRATEGY OF LATERAL-HEADING GUIDANCE LAW

From the point of view of the nominal flight trajectory design, the takeoff of a hypersonic aircraft is divided into three stages, and no lateral trajectory is designed for the three stages. Therefore, it is considered that in the nominal state, the lateral and heading movements should be in a balanced state. During the actual takeoff process, there is an initial position deviation and crosswind interference, so it is necessary to introduce rectifying guidance design.

2) DESIGN OF LATERAL-HEADING GUIDANCE LAW

The traditional PID strategy is adopted in the lateral direction guidance law, which takes the lateral position deviation, velocity and trajectory deviation angle as the controlled quantity, and the deviation from the runway center is fed back to the sideslip angle to generate guidance instructions for deviation correction. The expression is as follows:

$$\beta_c = k_1\Delta Y + k_2\Delta\dot{Y} + k_3\int \Delta Y \tag{24}$$

The block diagram of its guidance law is shown in the figure:

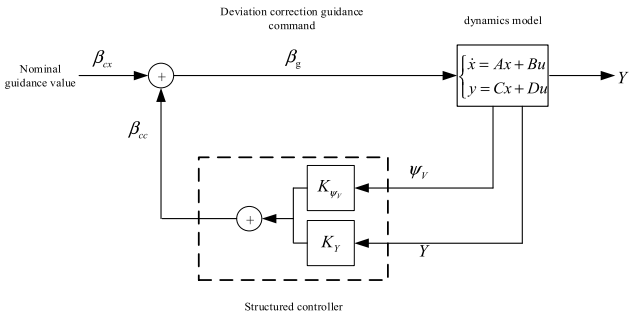

FIGURE 2. Yaw guidance block diagram.

IV. DESIGN OF ATTITUDE CONTROL LAW

The MPC approach is one of effective approaches to deal with model uncertainties and unknown disturbances, and provide the optimal tracking performance. The basic idea is to employ the system model to predict future states of the systems. State predictions are then used to determine future control moves while minimizing future errors and control effort.

A. DESIGN OF LONGITUDINAL ATTITUDE STABILITY CONTROL LAW BASED ON IMPC

1) MPC MODELING

With the help of Taylor's expansion, the following longitudinal discrete prediction model can be derived from attitude dynamic model of the RLVs [14], [15], [25].

$$\begin{pmatrix} \alpha(t+h) \\ \alpha(t+2h) \\ \alpha(t+3h) \\ \cdots \\ \alpha(t+nh) \end{pmatrix} = \begin{pmatrix} \alpha(t)+h\omega_z(t) \\ \alpha(t)+2h\omega_z(t) \\ \alpha(t)+3h\omega_z(t) \\ \cdots \\ \alpha(t)+nh\omega_z(t) \end{pmatrix} + \frac{1}{c}\begin{pmatrix} \frac{h^2}{2} & 0 & 0 & \cdots & 0 \\ \frac{h^2}{2}+h^2 & \frac{h^2}{2} & 0 & \cdots & 0 \\ \frac{h^2}{2}+2h^2 & \frac{h^2}{2}+h^2 & \frac{h^2}{2} & \cdots & 0 \\ \cdots & \cdots & \cdots & \cdots & 0 \\ \frac{h^2}{2}+(n-1)h^2 & \frac{h^2}{2}+(n-2)h^2 & \cdots & \cdots & \frac{h^2}{2} \end{pmatrix} \times \begin{pmatrix} u(t) \\ u(t+h) \\ u(t+2h) \\ \cdots \\ u(t+(n-1)h) \end{pmatrix} \tag{25}$$

The above predictive model can be reformulated as

$$\hat{y}(k) = \boldsymbol{y_0(k)} + \boldsymbol{bu(k)} \tag{26}$$

The following quadratic performance index function is chosen as:

$$J = \sum_{j=1}^{n}\left(\left[\hat{y}(k+j) - y_c(k+j)\right]^2 + Qu(k+j-1)^2\right) \tag{27}$$

where $\hat{y}(k+j) - yc(k+j)$ represents the tracking error of the step $k+j$ predicted in the step k, and $u(k+j-1)$ represents the control sequence at step. Q denotes weight coefficient to reflect the importance level of tracking error and consumed control energy, and n denotes the maximum predicted length at one time.

Considering of the optimization problem of the proposed performance index (27), the required MPC input can be obtained by the minimal principle:

$$\boldsymbol{u} = (\boldsymbol{Qb}^T\boldsymbol{b} + \boldsymbol{I})^{-1}\boldsymbol{Qb}^T(\boldsymbol{y_c} - \boldsymbol{y_0}) \tag{28}$$

Here, only the first value of the obtained optimal control input sequence is selected as the control torque required for the RLVs at this moment:

$$M_{zc} = [\,1 \quad 0 \quad \cdots \quad 0\,]\boldsymbol{u} \tag{29}$$

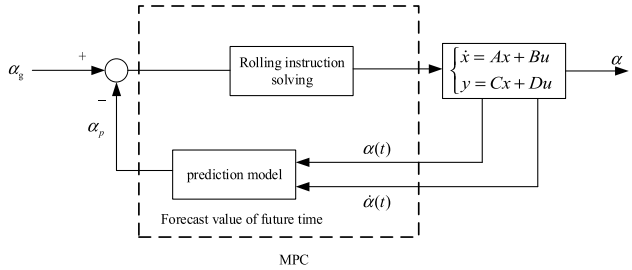

FIGURE 3. Longitudinal MPC strategy.

2) MPC VIA GROUND EFFECT PARAMETER IDENTIFICATION

In the ground effect area, the aerodynamic characteristics of RLVs are different from those outside the ground effect area. Due to the existence of the ground, the ground vortex is changed, the airflow velocity under the wing is reduced, and the pressure difference between the upper and lower wing surfaces is increased, thus the lift force of the wing is increased, the induced drag is decreased, the lift-drag ratio is increased, and the lift effect of the ground effect will form an additional bow moment, the rudder efficiency of the elevator will also increase to a certain extent. Outside the effective area, the influence of the ground effect has basically disappeared [26]. Therefore, the uncertainties of the moment and rudder efficiency should also be considered in the design of the controller.

Common methods to solve this problem are to design interval state estimator and sliding mode disturbance observer [27]–[32]. The method used here is to observe the uncertainty factor in real time and modify the MPC. Hence, the uncertainty factor is introduced to reflect the effect of ground effect on RLVs takeoff, and the modified model predictive controller is used to reflect the real situation of RLVs takeoff control more truly. The uncertainty factor K_F is determined as follows:

$$\begin{aligned} K_F &= \frac{\boldsymbol{u_R}}{\boldsymbol{u_T}} \\ \hat{\boldsymbol{y}}(k) &= \boldsymbol{y_0(k)} + \boldsymbol{bu(k)} \Rightarrow \hat{\boldsymbol{y}}(k) = \boldsymbol{y_0(k)} + K_F\boldsymbol{bu(k)} \\ \boldsymbol{u_R} &= \frac{d\boldsymbol{\omega_z}}{dt}Jz = K_F\boldsymbol{u_T} \\ \boldsymbol{u_T} &= \boldsymbol{u(k)} \end{aligned} \tag{30}$$

Among them, $\boldsymbol{u_R}$ the real aerodynamic pitch moment, $\boldsymbol{u_T}$ is the nominal control aerodynamic moment.

Considering the slow variation property of K_F, which can be treated as constant in one period. Therefore, the estimated value of K_F can be obtained by the following relationship.

$$K_F = \begin{cases} 1 & u_T = 0 \\ \dfrac{J_z \times \frac{\omega_z(i-1)-\omega_z(i-2)}{h} - M_F}{M_z(i-2)} & else \end{cases} \tag{31}$$

It is not difficult to derive from the equation (31) that the condition of IMPC is that the uncertainty factor K_F changes slowly and stably.

The control block diagram can be amended as follows:

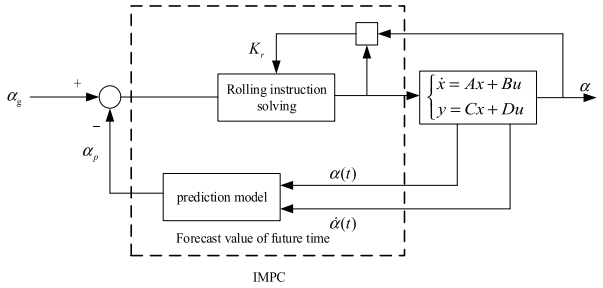

FIGURE 4. IMPC control flow chart.

B. DESIGN OF LATERAL-HEADING COUPLING MPC

1) COUPLING CONTROL STRATEGY OF TRANSVERSE-HEADING BASED ON HETEROGENEOUS MECHANISM COOPERATION

In the three-wheel running correction control, the available control mechanisms of the RLVs include rudder and front wheel steering. Affected by its working mechanism and motion state, the two types of control mechanisms have their own application scope and control effectiveness. When skating at a low speed, due to the limited aerodynamic efficiency of the rudder, the front wheel steering is mainly used for route / course control. As the skating speed accelerates, the front wheel transits from the grounded state to the ground and then to the ground, which causes the deflection center of the heading channel to change, and the steering efficiency of the front wheel is gradually weakened. Currently, with the increase of the speed, the steering control efficiency is gradually improved.

Actuator / torque distribution logic is speed related, this article considers low speed taxi is $V < V_1$, When the rudder has sufficient correction ability is $V > V_2$, when $V_1 \leq V \leq V_2$, Control torque distribution according to linear relationship. The front wheel actuator / torque distribution logic is as follows:

$$k_l = \begin{cases} 1 & V < V_1 \\ 1 - \dfrac{V - V_1}{V_2} & V_1 \leq V \leq V_2 \\ 0 & V > V_2 \end{cases} \tag{32}$$

During the ground running phase, the rolling moment includes the pneumatic rolling moment and the supporting force rolling moment. Because the supporting force has sufficient balance ability, the control of the rolling channel need not be discussed separately.

After the aircraft takes off, the landing gear is retracted. At this time, the correction of the lateral deviation depends entirely on the rudder, and the balance of the roll channel is achieved by the deflection of the aileron.

2) MPC MODELING

Considering the strong coupling effect between the yaw channel and roll channel, a coupled model predictive controller is designed by introducing the feedback of sideslip angle into the roll control channel to eliminate the coupling effect. Similar with the longitudinal case, the lateral discretization prediction model of RLVs can be obtained via Taylor's expansion [25], [14].

$$\begin{pmatrix} \beta(t+h) \\ \beta(t+2h) \\ \beta(t+3h) \\ \cdots \\ \beta(t+nh) \end{pmatrix} = \begin{pmatrix} \beta(t) - h\cos(\alpha(t))\omega_y(t) \\ \beta(t) - 2h\cos(\alpha(t))\omega_y(t) \\ \beta(t) - 3h\cos(\alpha(t))\omega_y(t) \\ \cdots \\ \beta(t) - nh\cos(\alpha(t))\omega_y(t) \end{pmatrix} + \frac{B_y}{Jy} \begin{pmatrix} u(t) \\ u(t+h) \\ u(t+2h) \\ \cdots \\ u(t+(n-1)h) \end{pmatrix}$$

$$\begin{pmatrix} \gamma_V(t+h) \\ \gamma_V(t+2h) \\ \gamma_V(t+3h) \\ \cdots \\ \gamma_V(t+nh) \end{pmatrix} = \begin{pmatrix} \gamma_V(t) + h\cos(\alpha(t))\omega_x(t) \\ \gamma_V(t) + 2h\cos(\alpha(t))\omega_x(t) \\ \gamma_V(t) + 3h\cos(\alpha(t))\omega_x(t) \\ \cdots \\ \gamma_V(t) + nh\cos(\alpha(t))\omega_x(t) \end{pmatrix} + k_3\beta(t) + \frac{C_x}{Jx} \begin{pmatrix} u(t) \\ u(t+h) \\ u(t+2h) \\ \cdots \\ u(t+(n-1)h) \end{pmatrix} \tag{33}$$

where B_y and C_x are as (34), shown at the bottom of the next page.

The above predictive model can be reformulated as

$$\begin{aligned} \hat{\boldsymbol{y}}_{\boldsymbol{1}}(\boldsymbol{k}) &= \boldsymbol{y}_{\boldsymbol{1_0}}(\boldsymbol{k}) + \boldsymbol{b_1 u_1}(\boldsymbol{k}) \\ \hat{\boldsymbol{y}}_{\boldsymbol{2}}(\boldsymbol{k}) &= \boldsymbol{y}_{\boldsymbol{2_0}}(\boldsymbol{k}) + \boldsymbol{b_2 u_2}(\boldsymbol{k}) \end{aligned} \tag{35}$$

The following quadratic performance index functions are chosen as:

$$\begin{aligned} J_1 &= \sum_{j=1}^{n} \left(\left[\hat{y}_1(k+j) - y_{1c}(k+j) \right]^2 + Q_1 u_1(k+j-1)^2 \right) \\ J_2 &= \sum_{j=1}^{n} \left(\left[\hat{y}_2(k+j) - y_{2c}(k+j) \right]^2 + Q_2 u_2(k+j-1)^2 \right) \end{aligned} \tag{36}$$

where $\left[\hat{y}_1(k+j) - y1_c(k+j)\right]$ and $\left[\hat{y}_2(k+j) - y2_c(k+j)\right]$ represent the tracking error of the step $k+j$ predicted in the step k in yaw and roll channel. $u_1(k+j-1)$ and $u_2(k+j-1)$ represent the control sequence at step in yaw and roll channel. Q_1 and Q_2 denote weight coefficient to reflect the importance level of tracking error and consumed control energy in yaw and roll channel, and n denotes the maximum predicted length at one time.

Where $K\beta$ is the coefficient of introducing side slip angle negative feedback to eliminate serious lateral coupling effect, and K_{F1}, K_{F2} are the jet interference factors of yaw and roll channel. Considering of the optimization problem of the

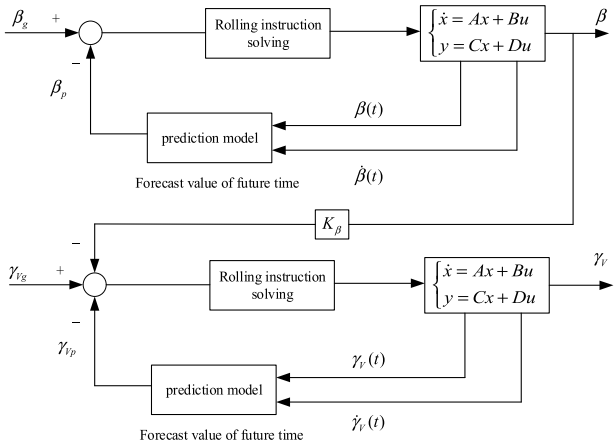

FIGURE 5. Lateral coupled IMPC strategy.

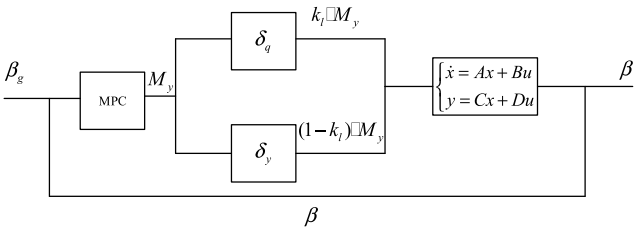

FIGURE 6. Control distribution diagram of heterogeneous actuators.

proposed performance index (28), the required MPC input can be obtained by the minimal principle:

$$\begin{aligned} \boldsymbol{u_1} &= (\boldsymbol{Q_1 b_1^T b_1} + \boldsymbol{I})^{-1} \boldsymbol{Q_1 b_1^T} (\boldsymbol{y1_c} - \boldsymbol{y1_0}) \\ \boldsymbol{u_2} &= (\boldsymbol{Q_2 b_2^T b_2} + \boldsymbol{I})^{-1} \boldsymbol{Q_2 b_2^T} (\boldsymbol{y2_c} - \boldsymbol{y2_0}) \end{aligned} \tag{37}$$

Here, only the first value of the obtained optimal control input sequence is selected as the control torque required for the RLVs at this moment:

$$\begin{aligned} M_{yc} &= [\,1 \quad 0 \quad \cdots \quad 0\,]\boldsymbol{u_1} \\ M_{xc} &= [\,1 \quad 0 \quad \cdots \quad 0\,]\boldsymbol{u_2} \end{aligned} \tag{38}$$

According to the above control strategy and control model, it can be concluded that the torque distribution logic and block diagram of the aircraft during the three-wheel rolling phase are as follows:

$$\begin{cases} M_y(\delta_q) = k_l M_y \\ My(\delta_y) = (1 - k_l) M_y \end{cases} \tag{39}$$

Remark: For a discrete MPC controller, it is equivalent to solving an LQR controller for the linearized system at each step, and this controller can always find a Lyapunov function, prove that the system is progressively stable in infinite time [34]. For nonlinear systems, the design of the MPC controller is an open question, and the proof of its stability will also be one of our follow-up research work.

V. SIMULATION RESULTS

The physical parameters and initial conditions of the aircraft are given

A. NOMINAL TRAJECTORY DESIGN

According to the takeoff strategy, set a safe flight altitude of 500m, and then climb at a constant pitch angle of 13° after leaving the ground, and simulate the whole process of the aircraft's taxiing takeoff section. The simulation results are as follows.

$$\boldsymbol{B_y} = \begin{pmatrix} \frac{h^2}{2} & 0 & 0 & \cdots & 0 \\ \frac{h^2}{2} - h^2\cos(\alpha(t)) & \frac{h^2}{2} & 0 & \cdots & 0 \\ \frac{h^2}{2} - 2h^2\cos(\alpha(t)) & \frac{h^2}{2} - h^2\cos(\alpha(t)) & \frac{h^2}{2} & \cdots & 0 \\ \cdots & \cdots & \cdots & \cdots & 0 \\ \frac{h^2}{2} - (n-1)h^2\cos(\alpha(t)) & \frac{h^2}{2} - (n-2)h^2\cos(\alpha(t)) & \cdots & \cdots & \frac{h^2}{2} \end{pmatrix}$$

$$\boldsymbol{C_x} = \begin{pmatrix} \frac{h^2}{2} & 0 & 0 & \cdots & 0 \\ \frac{h^2}{2} + h^2\cos(\alpha(t)) & \frac{h^2}{2} & 0 & \cdots & 0 \\ \frac{h^2}{2} + 2h^2\cos(\alpha(t)) & \frac{h^2}{2} + h^2\cos(\alpha(t)) & \frac{h^2}{2} & \cdots & 0 \\ \cdots & \cdots & \cdots & \cdots & 0 \\ \frac{h^2}{2} + (n-1)h^2\cos(\alpha(t)) & \frac{h^2}{2} + (n-2)h^2\cos(\alpha(t)) & \cdots & \cdots & \frac{h^2}{2} \end{pmatrix} \tag{34}$$

TABLE 1. Basic parameters list of hypersonic vehicles.

Symbol	Description	Value	Unit
c	Characteristic Length of RLVs	1.0186	m
S	Reference area	1.0375	m2
Jx	Roll moment of inertia	1637100	N·m
Jy	Yaw moment of inertia	1622889	N·m
Jz	Pitching moment of inertia	9233424	N·m
g	Gravitational acceleration	9.8	m/s2
m0	Initial mass	188769	kg
V0	Initial velocity	0	m/s
$\alpha 0$	Initial angle of attack	3	◦
$\theta 0$	Initial trajectory inclination	0	◦
$\vartheta 0$	Initial pitch angle	3	◦
H0	Initial height	0	m

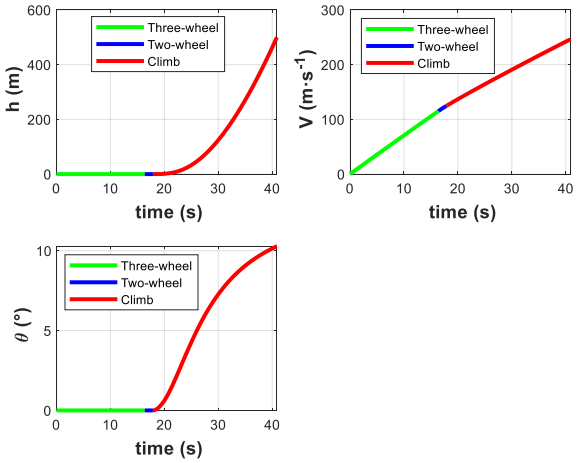

FIGURE 7. Nominal trajectory curve of altitude, speed, trajectory inclination.

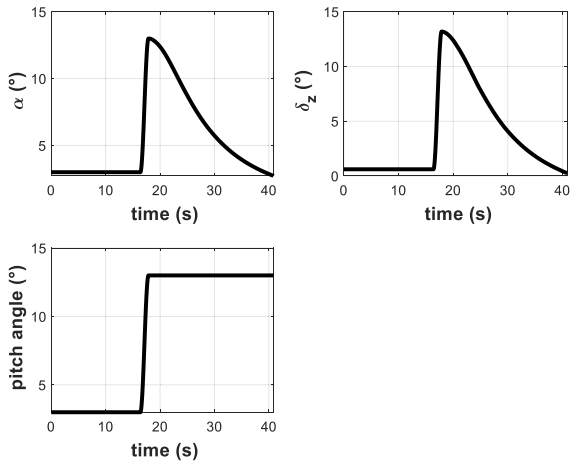

FIGURE 8. Nominal trajectory curve of angle of attack, elevator and pitch angle.

B. SIMULATION OF LONGITUDINAL CHANNEL

1) SIMULATION OF LONGITUDINAL GUIDANCE

Considering the influence of aerodynamic uncertainty during flight, this article considers the lift uncertainty and drag uncertainty separately. In the case of 10% uncertainty in lift or resistance, the TLC method is used to simulate compared. The simulation results considering lift uncertainty are as follows:

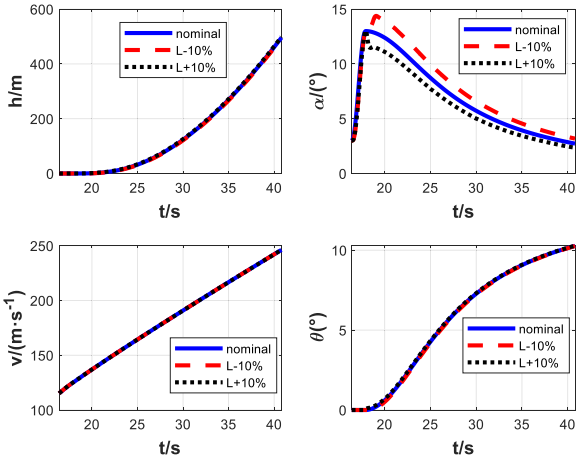

FIGURE 9. Guidance comparison simulation curve with 10% lift uncertainty.

Guidance simulation results considering resistance uncertainty are as follows

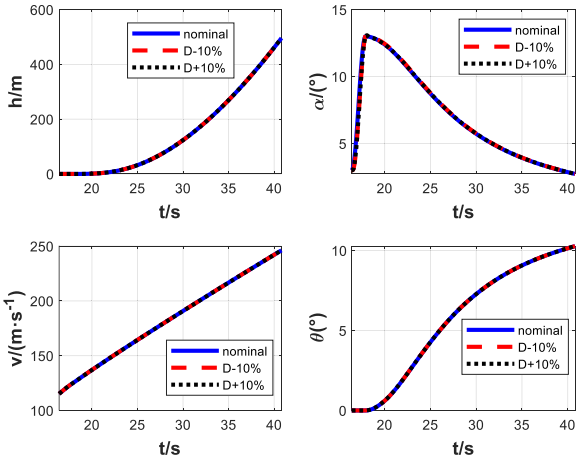

FIGURE 10. Guidance comparison simulation curve with 10% resistance uncertainty.

It can be seen from the simulation results that the TLC also has high guidance accuracy under the consideration of aerodynamic uncertainty. In the case of lift deflection, the trajectory inclination angle is greatly affected. Therefore, a large correction of the angle of attack is required to ensure the guidance accuracy of altitude and speed. When the drag is deflected, the acceleration is mainly affected, but the engine thrust is adjustable. Therefore, the accuracy of drag uncertainty is higher than that of lift uncertainty.

2) SIMULATION OF LONGITUDINAL GUIDANCE AND CONTROL

Under the consideration of changing the elevator tracking guidance instruction, the guidance period is 0.1s, and the control period is 0.01s. By employing the TLC and MPC control method, the simulation analysis is carried out under

the condition of considering the uncertainty of aerodynamic pitching moment. The simulation result is shown in the figures:

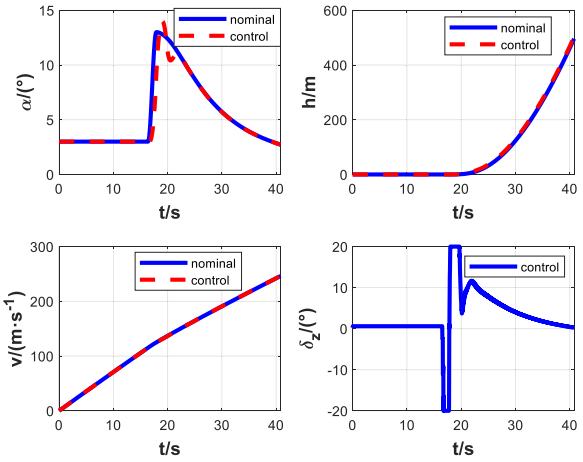

FIGURE 11. Comparison of the results of the guidance control simulation curve and the nominal trajectory when the pitching moment is reduced by 20%.

The simulation of pitching moment pull-up guidance and control is shown in the figure:

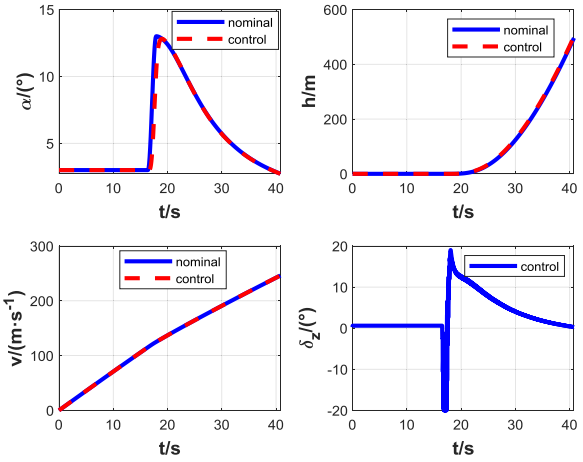

FIGURE 12. Comparison of the results of the guidance control simulation curve and the nominal trajectory when the pitching moment is added by 20%.

It can be seen from the simulation results that in the case of aerodynamic uncertainty, the trajectory linearization tracking guidance and MPC controller can still make RLVs reach the safe altitude with high accuracy even with the 20% increase of the pitching torque.

C. SIMULATION OF LATERAL-HEADING CHANNEL

1) SIMULATION OF LATERAL-HEADING GUIDANCE

Considering that there is a 2 m lateral deviation at the starting point of the three-wheel slide, the PID deviation correction guidance law is adopted, and the sideslip angle in the guidance link is taken as the control quantity. The guidance simulation starts from $V = 10m/s$, intending to verify the rapidity and effectiveness of correction. The simulation results of guidance are given below.

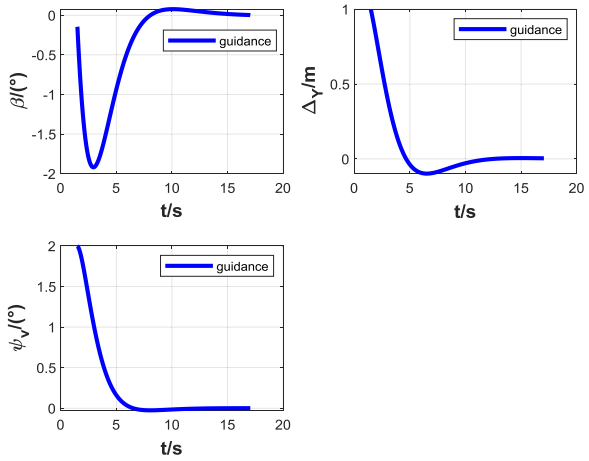

FIGURE 13. Simulation curve of deviation guidance when the initial position of the aircraft is 1m away from the centerline of the runway.

2) SIMULATION OF LATERAL-HEADING GUIDANCE AND CONTROL

The simulation mainly focuses on the design of uncertain factors. Uncertain factor 1, the lateral error between the aircraft body axis and the runway centre line at the initial position is 2 m; uncertain factor 2, when H=20m, a sudden crosswind of 5 m/s occurs, resulting in the sudden change of the sideslip angle. After two uncertain factors are added, the guidance period is 0.1s and the control period is 0.01s. Since there is no sudden change in the trajectory deflection angle and sideslip angle, the correction guidance is introduced from the initial state. The simulation results are as follows:

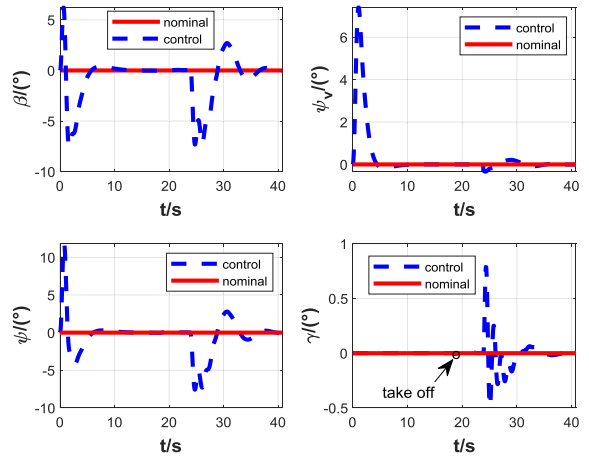

FIGURE 14. The simulation curve of the guidance control of the lateral-heading angle value after adding the uncertainty factor.

When RLVs is in the three-wheel rolling stage, in order to meet the conditions of rolling moment balance, the simulation results of the left and right main landing gear support forces are as follows

From the simulation results, it can be seen that the correction guidance scheme is feasible. For the initial position deviation given by the simulation, the joint correction can be performed through a heterogeneous structure. For the influence of crosswind after take-off, it also has the effect of

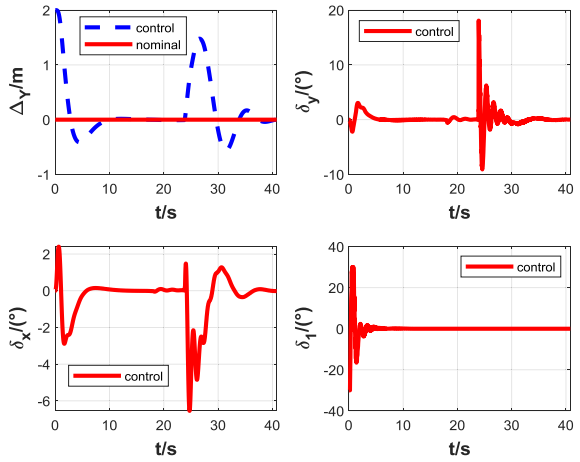

FIGURE 15. The simulation curve of the guidance control of the lateral position and control surface after adding the uncertainty factor.

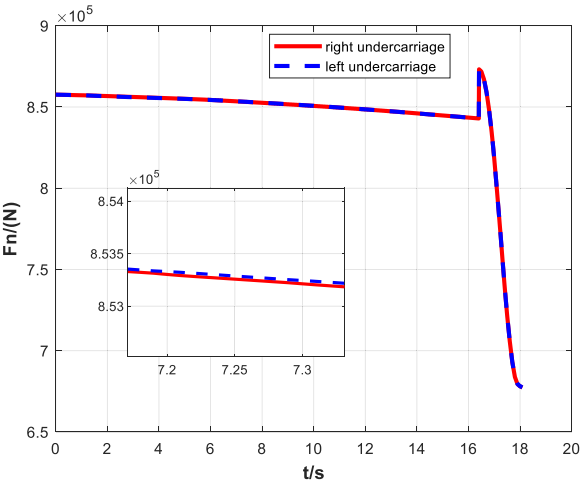

FIGURE 16. Main landing gear support-time curve.

attitude control and deviation correction. Finally, the influence of disturbance is eliminated, and the lateral deviation correction enhances the flight stability of the aircraft.

D. SIMULATION OF IMPC

Considering the ground effect, it can affect the maximum aerodynamic pitching moment of 15%. The height-related ground effect factor k is given below.

$$k = \begin{cases} 1.15 - 1.15 \times \dfrac{H - 20}{20} & H < 20 \\ 1 & H \geq 20 \end{cases} \tag{40}$$

The simulation results of comparison between IMPC control effect and MPC control effect are as follows:

It can be seen from the simulation results that the introduction of the ground effect influence factor into the real-time solution of control instructions can enlarge the control instruction solved by the MPC controller in the ground effect area. Compared to the control without considering the ground effect factor, it can be seen that the smaller rudder can achieve the same control effect. Based on this, when the ground effect is to reduce the aerodynamic torque, the MPC considering the

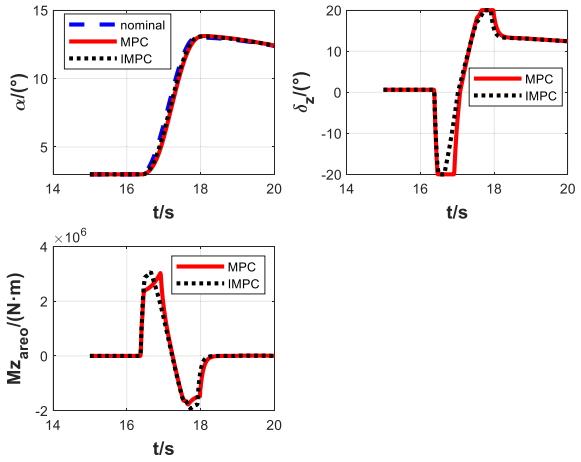

FIGURE 17. Aiming at the head-up process of the aircraft, the curves of the numerical simulation results of IMPC and MPC.

ground effect factor will increase the accuracy of the elevator deviation control.

VI. CONCLUSION

In this paper, a six-degree-of-freedom dynamic model of RLVs is established and the design and simulation of take-off guidance control are completed. The results show that the TLC guidance and MPC controller methods are effective in the guidance control during take-off. TLC guidance method can place poles of highly nonlinear systems at desired positions, the error between the predicted value and the guidance instruction of the future time is used in the MPC controller at the current moment to effectively suppress the overshoot, The rolling optimization idea is adopted to improve the accuracy of system control. The robustness of the system is further enhanced by the ways of online estimation of the uncertainty factor and the introduction of the sideslip angle into the roll channel. Moreover, it can be seen through simulation that the control logic of heterogeneous actuators based on speed distribution has a good effect in lateral correction.

REFERENCES

[1] J. Zhou, Y. Xiao, K. Liu, and W. She, "Preliminary analysis for a two-stage-to-orbit reusable launch vehicle," in *Proc. 20th AIAA Int. Space Planes Hypersonic Syst. Technol. Conf.*, Jul. 2015, pp. 1–21.

[2] D. Zhang, S. Tang, L. Cao, F. Cheng, and F. Deng, "Research on control-oriented coupling modeling for air-breathing hypersonic propulsion systems," *Aerosp. Sci. Technol.*, vol. 84, pp. 143–157, Jan. 2019, doi: 10.1016/j.ast.2018.10.014.

[3] C. Wei, X. Ju, F. He, and B. Lu, "Research on non-stationary control of advanced hypersonic morphing vehicles," in *Proc. 21st AIAA Int. Space Planes Hypersonics Technol. Conf.*, Mar. 2017, p. 2405.

[4] G. J. Gstattenbauer, M. E. Franke, and J. W. Livingston, "Cost comparison of expendable, hybrid, and reusable launch vehicles," in *Proc. Collection Tech. Papers-Space Conf.*, 2006, pp. 128–138.

[5] *Evaluation of the National Aerospace Initiative*, Air Force Sci. Technol. Board., Nat. Acad. Press, Washington, DC, USA, 2004. [Online]. Available: http://www.nap.edu

[6] P. W. Sacher. (2010). *The Engineering Design of Engine/Airframe Integration for the SAENGER Fully Reusable Space Transportation System*. [Online]. Available: http://www.dtic.mil/docs/citations/ADA592434?

[7] S. Weingertner, "SAENGER—The reference concept of the German hypersonics technology program," in *Proc. AIAA/DGLR 5th Int. Aerosp. Planes Hypersonic Technol. Conf.*, Munich, Germany, Nov. 1993, pp. 1–9.

[8] Q. J. Liu, "Research on attitude control technology of reentry stage of hypersonic vehicle," M.S. thesis, Nanjing Univ. Aeronaut. Astronaut., Jiangsu, China, 2011.
[9] Z. Feng and J. Zhou, "Design of multi-constrained robust attitude controller for hypersonic vehicle," *J. Astronaut.*, vol. 38, no. 8, pp. 839–846, 2017.
[10] F. Alberto, G. Guidotti, G. Rufolo, G. Malucchi, A. Denaro, F. Massobrio, S. Dussy, S. Mancuso, and G. Tumino, "The space rider programme: End user's needs and payload applications survey as driver for mission and system definition," *Acta Astron.*, vol. 152, pp. 534–541, Nov. 2018, doi: 10.1016/j.actaastro.2018.08.042.
[11] H. Mark, J. Aprea, B. Gallagher, and G. Sadlier, "A business analysis of a SKYLON-based European launch service operator," *Acta Astron.*, vol. 121, pp. 1–12, Apr./May 2016, doi: 10.1016/j.actaastro.2015.12.022.
[12] W. Wang, Z. Hou, X. Gao, and L. Chen, "Lowest-technical-merit design methodology of hypersonic cruise vehicle," *IEEE Access*, vol. 7, pp. 56480–56491, 2019, doi: 10.1109/ACCESS.2019.2913989.
[13] W. Wang, Z. Hou, S. Shan, and L. Chen, "Optimal periodic control of hypersonic cruise vehicle: Trajectory features," *IEEE Access*, vol. 7, pp. 3406–3421, 2019, doi: 10.1109/ACCESS.2018.2885597.
[14] X. Cheng, G. Tang, P. Wang, and L. Liu, "Predictive sliding mode control for attitude tracking of hypersonic vehicles using fuzzy disturbance observer," *Math. Problems Eng.*, vol. 2015, pp. 1–13, Feb. 2015, doi: 10.1155/2015/727162.
[15] W. R. van Soest, Q. P. Chu, and J. A. Mulder, "Combined feedback linearization and constrained model predictive control for entry flight," *J. Guid., Control, Dyn.*, vol. 29, no. 2, pp. 427–434, Mar. 2006, doi: 10.2514/1.14511.
[16] L. L. Ji, "Research on autonomous landing control technology of wheeled UAV," M.S. thesis, Nanjing Univ. Aeronaut. Astronaut., Jiangsu, China, 2012.
[17] D. F. Ning, W. G. Zhang, and N. Tian, "Modeling and control law design of UAV automatic takeoff system," *Comput. Meas. Control*, vol. 16, no. 1, pp. 66–67, 2008, doi: 10.16526/j.cnki.11-4762/tp.2008.01.005.
[18] C. F. Wu, B. Yan, and P. Y. Shao, "Research on control method of unmanned aerial vehicle takeoff based on fuzzy control," *J. Northwest Polytech. Univ.*, vol. 1, no. 1, pp. 33–39, 2015.
[19] S. Pradeep, "Nonlinear control of unmanned combat aircraft during takeoff," in *Proc. 40th AIAA Aerosp. Sci. Meeting Exhib.*, Aug. 2002, p. 250, doi: 10.2514/6.2002-250.
[20] O. Masahiro, Y. Yasuhiro, and H. Takashi, "Robust flight control law design for an automatic landing flight experiment," *Control Eng. Pratice*, vol. 7, no. 9, pp. 1143–1151, 1999, doi: 10.1016/s0967-0661(99)00085-4.
[21] X. Huang and Z. M. Yang, "Research on MPC-based intelligent car trajectory tracking controller," *Light Ind. Sci. Technol.*, vol. 35, no. 10, pp. 41–42, 2019.
[22] B. Qiu, G. Wang, Y. Fan, D. Mu, and X. Sun, "Adaptive course control-based trajectory linearization control for uncertain unmanned surface vehicle under rudder saturation," *IEEE Access*, vol. 7, pp. 108768–108780, 2019, doi: 10.1109/ACCESS.2019.2933405.
[23] M. C. Mickle and J. J. Zhu, "Skid-to-turn control of the APKWS missile using trajectory linearization technique," in *Proc. Amer. Control Conf.*, Arlington, TX, USA, 2001, pp. 3346–3351, doi: 10.1109/ACC.2001.946145.
[24] X. F. Wu, Y. Liu, and J. J. Zhu, "Design and real time testing of a trajectory linearization flight controller for the quanser UFO," in *Proc. Amer. Control Conf.*, Denver, CO, USA, 2003, pp. 3913–3918, doi: 10.1109/ACC.2003.1240447.
[25] W. S. Xiao and Z. Jun, "Nonlinear predictive attitude control of hypersonic vehicle," *J. Ballistics*, vol. 21, no. 4, pp. 42–46, 2009, doi: 10.1109/ICICSE.2009.69.
[26] M. Li and N. Zhang, "Analysis of ground effect of V-tail aircraft," in *Proc. Int. Conf. Aerosp. Eng. Inf. Technol. (AEIT)*, 2012, pp. 248–252.
[27] I. Ullah and H.-L. Pei, "Sliding mode tracking control for unmanned helicopter using extended disturbance observer," *Arch. Control Sci.*, vol. 29, no. 1, pp. 169–199, 2019.
[28] I. Ullah and H.-L. Pei, "Fixed time disturbance observer based sliding mode control for a miniature unmanned helicopter hover operations in presence of external disturbances," *IEEE Access*, vol. 8, pp. 73173–73181, 2020.
[29] A. Khan, W. Xie, and L.-W. Liu, "Set-membership interval state estimator design using observability matrix for discrete-time switched linear systems," *IEEE Sensors J.*, vol. 20, no. 11, pp. 6121–6129, Jun. 2020.
[30] H. Yang and H. Pei, "Approximate dynamic inversion for nonaffine nonlinear systems with high-order mismatched disturbances and actuator saturation," *IEEE Access*, vol. 8, pp. 26247–26256, 2020.
[31] A. Khan and W. Xie, "Interval state estimator design using the observability matrix for multiple input multiple output linear time-varying discrete-time systems," *IEEE Access*, vol. 7, pp. 167566–167576, 2019.
[32] A. Khan, W. Xie, and L. Zhang, "Interval state estimation for linear time-varying (LTV) discrete-time systems subject to component faults and uncertainties," *Arch. Control Sci.*, vol. 20, no. 2, pp. 289–305, 2019.
[33] Y. Liu, X. Wu, J. J. Zhu, and J. Lew, "Omni-directional mobile robot controller design by trajectory linearization," in *Proc. 29th Amer. Control Conf.*, Denver, CO, USA, Jun. 2003, pp. 3423–3428, doi: 10.1109/ACC.2003.1244061.
[34] D. Q. Mayne, J. B. Rawlings, C. V. Rao, and P. O. M. Scokaert, "Constrained model predictive control: Stability and optimality," *Automatica*, vol. 36, no. 6, pp. 789–814, Jun. 2000.

SHUAIBIN AN received the B.S. degree in engineering from Dalian Maritime University, in 2019. He is currently pursuing the M.S. degree in aerospace science and technology with the Dalian University of Technology. His research interest includes flight guidance and control.

KAI LIU (Member, IEEE) received the B.S. degree in information and computing science from Jilin University, China, in 2007, and the Ph.D. degree from the Harbin Institute of Technology, China, in 2013. He is currently an Associate Professor with the Dalian University of Technology. His research interest includes flight guidance and control.

YAZHUO FAN received the B.S. and M.S. degrees from the Nanjing University of Aeronautics and Astronautics, China, in 2010 and 2013, respectively. He is currently a Senior Engineer with the Beijing Aerospace Technology Institute. His research interests include guidance and control technology of air and space vehicles.

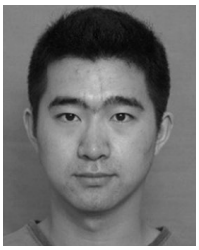

JIAN GUO received the B.S., M.S., and Ph.D. degrees from the Harbin Institute of Technology, China, in 2007, 2009, and 2014, respectively. He is currently working with the Beijing Aerospace Technology Institute. His research interests include spacecraft attitude dynamics and control, spacecraft guidance and navigation, and saturation control theory.

ZHIYONG SHE received the B.S., M.S., and Ph.D. degrees from the Harbin Institute of Technology, China, in 2004, 2006, and 2010, respectively. He is currently working with the Beijing Aerospace Technology Institute. His main research interest includes advanced guidance technology for hypersonic vehicles.